


# Investigation of Several Interpolation Functions for Unstructured Meshes in Conjunction with Compositional Reservoir Simulation


Bruno Ramon Batista Fernandes , Francisco Marcondes & Kamy Sepehrnoori

To cite this article: Bruno Ramon Batista Fernandes , Francisco Marcondes & Kamy Sepehrnoori (2013) Investigation of Several Interpolation Functions for Unstructured Meshes in Conjunction with Compositional Reservoir Simulation, Numerical Heat Transfer, Part A: Applications, 64:12, 974-993, DOI: [10.1080/10407782.2013.812006](https://doi.org/10.1080/10407782.2013.812006)


To link to this article: <https://doi.org/10.1080/10407782.2013.812006>

 Published online: 11 Sep 2013.

 Submit your article to this journal [↗](#)

 Article views: 110

 View related articles [↗](#)

 Citing articles: 5 View citing articles [↗](#)

## INVESTIGATION OF SEVERAL INTERPOLATION FUNCTIONS FOR UNSTRUCTURED MESHES IN CONJUNCTION WITH COMPOSITIONAL RESERVOIR SIMULATION

**Bruno Ramon Batista Fernandes<sup>1</sup>, Francisco Marcondes<sup>2</sup>, and Kamy Sepehrnoori<sup>3</sup>**

<sup>1</sup>Laboratory of Computational Fluid Dynamics, Federal University of Ceará, Campus do Pici, Ceará, Brazil

<sup>2</sup>Department of Metallurgical Engineering and Material Science, Federal University of Ceará Campus do Pici, Ceará, Brazil

<sup>3</sup>Department of Petroleum and Geosystems Engineering, The University of Texas at Austin, Austin, USA

*One of the key parameters in numerical simulation of fluid flow problems is the interpolation function used for adjusting the numerical value from the position where it is evaluated to the interface of the control volumes; for instance, if the finite-volume method is employed. In this article, we present an investigation of several interpolation functions in conjunction with the element based finite-volume method (EbFVM) using unstructured triangular meshes. We investigate the mass weighted upwind (MWU) and a modified version of this method, the upwind scheme, a streamline based upwind scheme, and a limited second order upwind scheme. These interpolation functions are implemented in a compositional simulator using vertex cell unstructured grids. The accuracy of these interpolation functions are evaluated for several case studies. For some of them, we also compare the results with the available analytical solutions.*

### 1. INTRODUCTION

Interpolation functions are important key parameters for numerical methods, such as finite difference, finite element method, and finite-volume method. The way the physical properties are interpolated by the interpolation function will determine the necessary mesh refinement, and can also originate numerical dispersion or physical oscillations and other type of errors. Hence, the use of interpolation function that can take into account the correct variation of fluid flow and discontinuities can reduce the computational time in order to obtain accurate numerical solutions. Several interpolation functions have been developed in previous decades.

Received 25 February 2013; accepted 8 May 2013.

Address correspondence to Francisco Marcondes, Department of Metallurgical Engineering and Material Science, Federal University of Ceará Campus do Pici, Bloco 729 Fortaleza, P.O. Box 12. 144, Ceará 60440-554, Brazil. E-mail: marcondes@ufc.br

## NOMENCLATURE

$A$	area, $m^2$	$\bar{V}_{ik}$	partial molar volume, $m^3/mol$
$Acc$	accumulation term	$u$	Cartesian velocity in x direction, $m/s$
$F$	advective plus diffusive transport	$v$	Cartesian velocity in y direction, $m/s$
$c_f$	rock compressibility, $Pa^{-1}$	$x$	phase mole fraction
$d$	distance, $m$	$z$	overall composition
$D'$	virtual vertex	$\alpha$	mass weighting factor
$f$	fugacity, $Pa$	$\Delta$	any physical property evaluated at the vertex
$\bar{K}$	absolute permeability tensor, $m^2$	$\delta$	any physical property evaluated at the interface
$\bar{K}_{ij}$	dispersion tensor, $m^2/s$	$\xi$	mole density, $mol/m^3$
$k_r$	relative permeability	$\phi$	porosity
$N$	number of moles per bulk volume, $mol/m^3$	$\lambda$	phase mobility, $(Pa.s)^{-1}$
$N_i$	linear shape function	$\Phi$	hydraulic potential, $Pa$
$N_e$	total number of elements	$\Psi$	nonlinear function of successive slope ratio
$N_v$	total number of vertices	$\gamma$	specific gravity, $Pa/m$
$n_e$	number of components	$\mu$	viscosity, $Pa.s$
$n_p$	number of phases		
$P$	Pressure, $Pa$	<b>Superscripts</b>	
$q$	well volumetric rate, $mol/s$	0	property evaluated at the previous time
$r$	successive slope ratio		
$S$	saturation or binary flux direction for MWU and MMWU schemes	<b>Subscripts</b>	
$t$	time, $s$	$i$	control volume, vertex, or component
$V_b$	bulk volume, $m^3$	$j$	phase
$V_p$	pore volume, $m^3$	$w$	water component
$V_t$	total fluid volume, $m^3$	$r$	reference phase

Some upwind interpolation schemes were designed for advection and diffusion problems by Baliga and Patankar [1]. Among them, is the exponential approach; the exponential approach is achieved using exponential shape functions in the direction of average velocity of the element. This scheme is called flow-oriented interpolation (FLO). Later, Prakash [2] proposed another shape function for FLO taking in account the source terms; this was called flow-oriented interpolation with source terms (FLOS) and was shown to be exact solutions of certain restricted cases. Other interpolation functions were developed with the goal of obtaining a better upwind interpolation for skewed grids. The skew upwind was first proposed by Raithby [3, 4] for regular grids. Hassan et al. [5] constructed the skew upwind for unstructured triangular meshes. Schneider and Raw [6] applied the skew upwind scheme for quadrilateral meshes. Swaminathan and Voller [7, 8] extended the streamline upwind Petrov-Galerkin (SUPG) scheme of Brooks and Hughes [9] from the finite element method (FEM) to the EbFVM approach. They called this scheme streamline upwind control volume (SUCV). This scheme uses the streamline to evaluate the upwind influence. Hurtado et al. [10] improved the 2-D MWU (mass weighted upwind) scheme for quadrilateral elements using a modified weighting factor. A more complete study about this new family of positive coefficient (MWU) scheme was presented in reference [11].

Van Leer [12] developed the first higher-order scheme, showing that the monotonicity for one dimension can be preserved by application of a flux-limiter that may be able to capture the flow discontinuity. The principles of this monotonicity preserving were later introduced by Harten [13] as the total variation diminishing (TVD) property. The TVD region was formulated by Sweby [14] who proved that the Van Leer's limiter, the Roe's limiter [15], and the Chakravarthy and Osher limiter [16] follow the TVD definition. Sweby [14] also showed that the Lax-Wendroff [17] and the Warming-Beam [18] schemes do not follow the TVD definition.

Several schemes have adapted the TVD interpolation function from structured grids to unstructured grids [19–26]. All of the aforementioned works are based on cell-center grids. Although some authors suggest that the scheme would also work for cell-vertex grids, they were all constructed and applied to cell-center unstructured grids. Therefore, to the best of our knowledge, TVD interpolation function has not yet been used in conjunction with cell-vertex unstructured meshes. In this work, we investigate the upwind, the mass weight upwind (MWU) and a modified version of this scheme (MMWU), the upwind scheme, a streamline based upwind scheme, and a second order TVD scheme. These interpolation functions are implemented in an in-house compositional reservoir simulator called UTCOMP [27, 28]. UTCOMP was developed at the Center for Petroleum and Geosystems Engineering at The University of Texas at Austin for the simulation of enhanced recovery processes. UTCOMP is an IMPEC, multiphase/multi-component compositional equation of state simulator which can handle the simulation of several enhanced oil recovery processes.

## 2. PHYSICAL MODEL

Isothermal, multi-component, multiphase fluid flow in a porous medium can be described using three types of equations: the component-material balance equation, phase equilibrium equation, and equation for constraining phase saturations and component concentrations [27, 28].

The material balance equation for the  $i$ th component for a full symmetric permeability tensor using the Einstein notation can be written as follows.

$$\frac{\partial(\phi N_i)}{\partial t} - \nabla \cdot \left[ \sum_{j=1}^{n_p} \xi_j x_{ij} \lambda_j \bar{K} \cdot \nabla \Phi_j + \phi \sum_{j=1}^{n_p} \xi_j S_j \bar{K}_{ij} \nabla x_{ij} \right] - \frac{q_i}{V_b} = 0 ; i = 1, 2, \dots, n_c \quad (1)$$

In Eq. (1),  $n_c$  is the number of hydrocarbon components,  $n_p$  is the number of phases present in the reservoir,  $\phi$  is the porosity,  $N_i$  is the moles of the  $i$ th component per unit of volume,  $\xi_j$  and  $\lambda_j$  are the molar density and relative mobility of the  $j$ th phase, respectively,  $x_{ij}$  is the molar fraction of the  $i$ th component in the  $j$ th phase,  $\bar{K}$  is the absolute permeability tensor,  $\bar{K}_{ij}$  is physical dispersion tensor,  $q_i$  is the molar flow rate of the component  $i$  due to well injection/production, and  $V_b$  is a volume of control-volume that could contain a well.  $\Phi_j$  is the potential of the  $j$ th phase and is given by the following.

$$\Phi_j = P_j - \gamma_j Z \quad (2)$$

Where  $P_j$  denotes the pressure of the  $j$ th phase and  $Z$  is depth, which is positive in a downward direction.

The first partial derivative of the total Gibbs free energy with respect to the independent variables gives the equality of component fugacities among all phases.

$$f_i = f_i^j - f_i^r = 0 \quad ; \quad i = 1, \dots, n_c \quad ; \quad j = 2, \dots, n_p \quad (3)$$

In Eq. (3),  $f_i^j = \ln(x_{ij} \phi_{ij})$ , where  $\phi_{ij}$  is the fugacity coefficient of component  $i$  in the  $j$ th phase,  $r$  denotes the reference phase, and  $n_c$  is the number of components excluding the water. The restriction of the molar fraction is used to obtain the solution of Eq. (3).

$$\sum_{i=1}^{n_c} x_{ij} - 1 = 0, \quad j = 2, \dots, n_p \quad ; \quad \sum_{i=1}^{n_c} \frac{z_i (K_i - 1)}{1 + \nu (K_i - 1)} = 0 \quad (4)$$

Where  $z_i$  is the overall molar fraction of the  $i$ th component,  $K_i$  is the equilibrium ratio for the  $i$ th component, and  $\nu$  is the mole fraction of the gas phase in the absence of water. The closure equation comes from the volume constraint, i.e., the available pore volume of each cell must be filled by all phases present in the reservoir. This constraint gives rise to the following equation.

$$\sum_{j=1}^{n_p} S_j = 1 \quad (5)$$

In UTCOMP simulator, the unknown primary variables are water pressure  $P_w$ ,  $N_1, \dots, N_{n_c}$ , and  $N_w$ . The water pressure is obtained through a volume balance and is given by

$$\left( \phi^0 c_f - \frac{1}{V_b} \frac{\partial V_t}{\partial P} \right) \frac{\partial P}{\partial t} = \sum_{k=1}^{n_c} \bar{V}_{tk} \sum_{j=1}^{n_p} \left( \vec{\nabla} \cdot x_{kj} \xi_j \frac{k_{rj}}{\mu_j} \bar{K} \cdot \vec{\nabla} \Phi_j + \vec{\nabla} \cdot \phi \xi_j S_j \bar{K}_{kj} \nabla x_{kj} \right) + \sum_{k=1}^{n_c} \bar{V}_{tk} \frac{q_k}{V_b} \quad (6)$$

In this work, an implicit pressure, explicit composition (IMPEC) formulation [29] is used to solve a set of nonlinear equations. In this formulation, the pressure is solved at the new time level using all other variables at the old time level. The new pressure is used to evaluate the mole balance, and then a flash calculation is performed to evaluate the amount and compositions of phases at the new time-step.

### 3. NUMERICAL DISCRETIZATION

In our work, the approximate equations are obtained by using the EbFVM. In the EbFVM, each element is divided into sub-elements, as shown in Figure 1. The conservation equations and the pressure equation, Eqs. (1) and (6), need to be

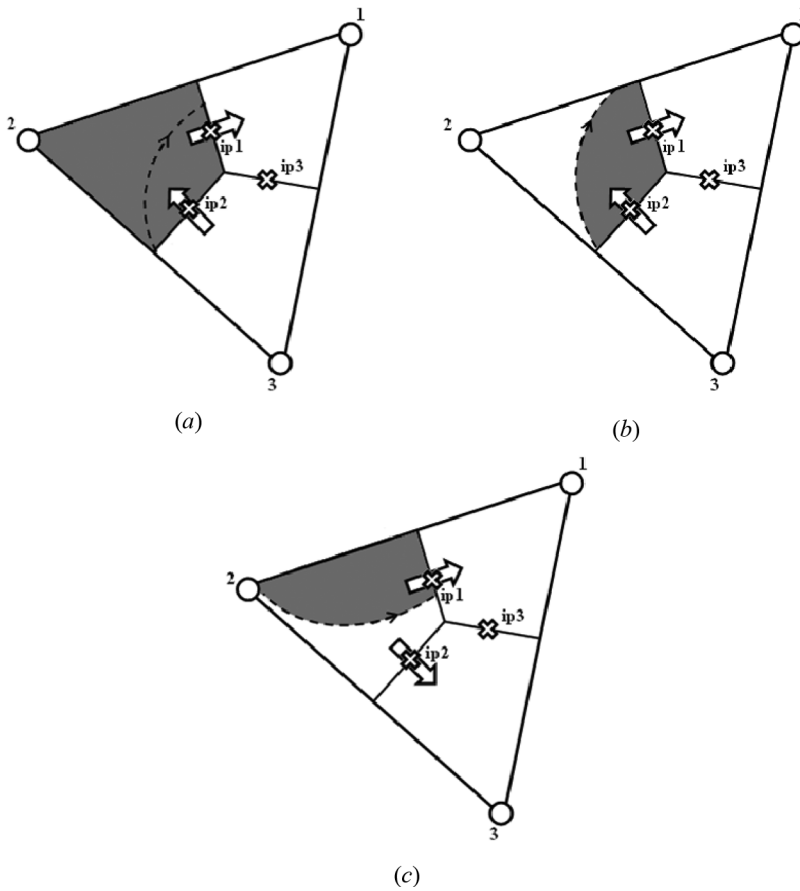


**Figure 1.** Sub-control volumes and possible situations for fluid flow convective out of ip1. (a) Physical property interpolated between vertex 2; and ip2 (b) physical property interpolated from ip2 (c) physical property interpolated from vertex.

integrated for each sub-control volume. Here, except for case study 1 of the results section, we have used only triangular elements. Figure 1 presents the sub-control volumes and integration points for the advective and diffusive terms. Integrating each term of Eq. (1), for instance, in space and time for each sub-control volume, and applying the Gauss theorem for the advective and dispersion terms, we obtain the following.

$$\int_{t,V} \frac{\partial \phi N_k}{\partial t} dt dV = \int_{t,A} \left( \sum_{j=1}^{n_p} x_{kj} \xi_j \frac{k_{rj}}{\mu_j} \bar{\mathbf{K}} \cdot \bar{\nabla} \Phi_j + \phi \xi_j S_j \bar{\mathbf{K}}_{kj} \nabla x_{kj} \right) \cdot \bar{\mathbf{dA}} dt + \int_{t,V} \frac{q_k}{V_b} dt dV, \quad k = 1, n_c \tag{7}$$

Performing the integration of first and second terms of Eq. (7), and evaluating the fluid properties through an explicit procedure, the following equations for the mentioned terms are obtained.

$$Acc_{m,i} = V_{scv_{m,i}} \left( \left( \frac{\phi N_m}{\Delta t} \right)_i - \left( \frac{\phi N_m}{\Delta t} \right)_i^o \right) \quad ; \quad m = 1, N_v \quad ; \quad i = 1, \dots, n_c \quad (8)$$

$$F_{m,i} = \int_A \sum_{j=1}^{n_p} \left( \lambda_j \xi_j x_{ij} \bar{K} \cdot \nabla \Phi_j - \phi \xi_j S_j K_{ij} \cdot \nabla x_{ij} \right) \cdot \overrightarrow{dA}$$

$$= \int_A \left( \sum_{j=1}^{n_p} \xi_j^0 x_{ij}^0 \lambda_j^0 K_{nl} \frac{\partial \Phi_j}{\partial x_l} - \phi \xi_j^0 S_j^0 K_{ijnl} \frac{\partial x_{ij}}{\partial x_l} \right) dA_n \quad m = 1, N_e \quad ; \quad n, l = 1, 2 \quad (9)$$

In the above equations  $N_v$  and  $N_e$  denote the number of vertices and number of elements of the grid, respectively. A similar procedure is performed to the pressure equation.

Inserting Eqs. (8) and (9) into Eq. (7), the following equation for each element is obtained.

$$Acc_{m,i} + F_{m,i} + q_i = 0 \quad ; \quad m = 1, \dots, N_e \quad ; \quad i = 1, \dots, n_c + 1 \quad (10)$$

Equation (10) denotes the conservation for each sub-control volume of each element. Now, it is necessary to assemble the equation of each control volume for obtaining the contribution of each sub-control volume that shares the same vertex. This process is similar to the assembling of the stiffness global matrix in the finite element method. Further details of the methodology just described can be found in Cordazzo [30] and Marcondes and Sepehrnoori [31, 32].

#### 4. INTERPOLATION SCHEMES

Here, we present the mass weighted upwind scheme (MWU), a modified version of the MWU scheme (MMWU), the streamline upwind scheme (SUCV) and a TVD scheme.

##### 4.1. Mass Weighted Upwind Scheme

The MWU scheme ensures that the convective property carried out of the control volume is equal or smaller than the one convected into the control volume. This condition ensures that the coefficients of the linear system being solved are always positive. As shown in Figure 1, for the convective flow carried at integration point 1 (ip1), three situations can occur. The first one is shown in Figure 1a, where the inflow into sub-control volume 2 (ip2) is smaller than the one carried out through ip1. For this situation, the property at ip1 should be interpolated between the ones at vertex 2 and ip1. The situation presented in Figure 1b is similar to Figure 1a, but now the outflow through ip1 is smaller than the inflow through ip2. For this case, the

property at ip1 should be equal to the one at ip2. The last case is presented in Figure 1c. For this case, the property at ip1 should be equal to the one at vertex 2.

Considering a generic physical property at the integration point ( $\delta$ ), all three cases illustrated in Figure 1 can be written as follows.

$$\delta_1 = (1 - \alpha_{12})\Delta_2 + \alpha_{12}\delta_2 \quad (11)$$

Where  $\Delta$  denote a property evaluated at vertex, and  $\alpha_{12}$  is the MINMOD function of the mass flow ratio defined as follows.

$$\alpha_{ij} = \max\left(0, \min\left(1, \frac{\dot{m}_j}{\dot{m}_i}\right)\right) \quad (12)$$

Three other possibilities are possible when the flux is convective into ip1. Now, the property at ip1 can be a function of vertex 1 or ip3. All six possibilities can be summarized as follows.

$$\delta_1 = (1 - S_1)[(1 - \alpha_{12})\Delta_2 + \alpha_{12}\delta_2] + S_1[(1 - \alpha_{14})\Delta_1 + \alpha_{14}\delta_3] \quad (13)$$

where,

$$S_i = \max\left(0, \frac{|\dot{m}_i|}{\dot{m}_i}\right) \quad (14)$$

For triangle elements, a set of three equations and three variables for  $\delta$  in each element is obtained.

$$\begin{aligned} \delta_1 &= (1 - S_1)[(1 - \alpha_{12})\Delta_2 + \alpha_{12}\delta_2] + S_1[(1 - \alpha_{13})\Delta_1 + \alpha_{13}\delta_3] \\ \delta_2 &= (1 - S_2)[(1 - \alpha_{23})\Delta_3 + \alpha_{23}\delta_3] + S_2[(1 - \alpha_{21})\Delta_2 + \alpha_{21}\delta_1] \\ \delta_3 &= (1 - S_3)[(1 - \alpha_{31})\Delta_1 + \alpha_{31}\delta_1] + S_3[(1 - \alpha_{32})\Delta_3 + \alpha_{32}\delta_2] \end{aligned} \quad (15)$$

## 4.2. Modified Mass Weight Upwind Scheme

In order to ensure that the influence of upwind vertex will cease only when the mass flow ratio goes to infinity, Hurtado et al. [10] proposed a modified equation to the  $\alpha$  coefficient given in Eq. (12). The new function for this coefficient is given by the following.

$$\alpha_{ij} = \max\left(0, \frac{\frac{\dot{m}_j}{\dot{m}_i}}{1 + \frac{\dot{m}_j}{\dot{m}_i}}\right) \quad (16)$$

## 4.3. Streamline Upwind Control-Volume

The streamline upwind uses the phase velocity at each control volume face. The phase velocity components for a 2-D porous medium is given by the following.



$$\begin{aligned}
 u_{j,ip} &= -K_{xx} \frac{k_{rj}}{\mu_j} \frac{\partial \Phi_j}{\partial x} \Big|_{ip} - K_{xy} \frac{k_{rj}}{\mu_j} \frac{\partial \Phi_j}{\partial y} \Big|_{ip} \\
 v_{j,ip} &= -K_{yx} \frac{k_{rj}}{\mu_j} \frac{\partial \Phi_j}{\partial x} \Big|_{ip} - K_{yy} \frac{k_{rj}}{\mu_j} \frac{\partial \Phi_j}{\partial y} \Big|_{ip}
 \end{aligned}
 \tag{17}$$

The velocity is used to compute a linear streamline at the integration point. The point on the edge of the element which the streamline crosses upstream the flow is used as the upwind point. Figure 2 presents an illustration of such a case for the integration point 2 (ip2). Therefore, the value of the physical property is calculated through a linear combination of the vertex values where the interception occurs. For the situation showed in Figure 2, we have the following.

$$\delta_2 = \frac{d_1}{d_1 + d_2} \Delta_2 + \frac{d_2}{d_1 + d_2} \Delta_3
 \tag{18}$$

Some spurious oscillations can occur when this interpolation function is used due to the inclusion of some downstream vertices [33, 34]. As shown in Figure 2, the vertex 2 is included into the linear interpolation even though a downstream point. Although the contribution can be small, it can lead to oscillations when a discontinuity arises due to a large jump in the value. For solving this issue, the downstream points are removed and the scheme is reduced to an upwind scheme.

**4.4. Second-Order TVD Scheme**

For TVD schemes, the flux-limiter can be interpreted as a switch between lower and higher order schemes to ensure a monotonic solution. The expression for a property at the integration point is defined by Darwish and Moukalled [21] as follows.

$$\delta_f = \Delta_C + \psi(r_f) \frac{(\Delta_D - \Delta_C)}{2}
 \tag{19}$$

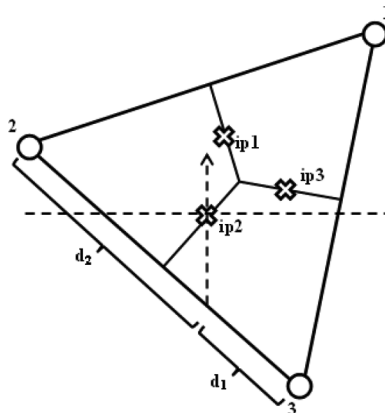


**Figure 2.** Illustration of streamline crossing the edge formed by vertices 2 and 3.

Where subscripts  $C$  and  $D$  denote the upwind and downwind control volumes, respectively, and  $\psi$  is a nonlinear function of the successive slope ratios ( $r_{ip}$ ) to control the second order contribution. The successive slope ratios are defined by Darwish and Moukalled [21] as follows.

$$r_f = \frac{2\vec{\nabla}\Delta_C \cdot \Delta\vec{r}_{CD} - (\Delta_D - \Delta_C)}{\Delta_D - \Delta_C} \quad (20)$$

Where  $\vec{\nabla}\Delta_C$  is the upwind vertex gradient, and  $\Delta\vec{r}_{CD}$  is the distance vector between the upwind and downwind vertices.

In the case of a cell-center scheme, the downwind property is formally the control volume that shares the face with the upwind vertex. Although this is also true for the EbFVM approach, the control volume face is too far from middle distance between the upwind and downwind vertices. Therefore, the mean value that would be evaluated at the face, which yields a central difference scheme, is not a good approach. One can substitute the downwind property into Eq. (19) for a virtual downwind ( $D'$ ) vertex property, and then substitute it by the face value evaluated through the shape functions considering it a central difference scheme.

$$\delta_f^{CDS} = \frac{(\Delta_{D'} + \Delta_C)}{2} \quad (21)$$

Thus,

$$\Delta_{D'} = 2\delta_f^{CDS} - \Delta_C \quad (22)$$

where,

$$\delta_f^{CDS} = \sum_{i=1}^{n_{ve}} N_i \Delta_i \quad (23)$$

Substituting Eq. (23) into Eq. (19), we obtain the following.

$$\delta_f = \Delta_C + \psi(r_f) (\delta_f^{CDS} - \Delta_C) \quad (24)$$

The face CDS value minus the upwind node value can also be written as a function of the face gradient as follows:

$$(\delta_f^{CDS} - \Delta_C) = \vec{\nabla}\delta_f \cdot \Delta\vec{r}_{CF} \quad (25)$$

Finally,

$$\delta_f = \Delta_C + \psi(r_f) \vec{\nabla}\delta_f \cdot \Delta\vec{r}_{CF} \quad (26)$$

The face gradient can be evaluated using the shape functions. The slope ratio needs to be adjusted as well. Substituting Eqs. (22) and (25) into Eq. (20), and substituting the distance vector,  $\Delta\vec{r}_{CD}$  by  $\Delta\vec{r}_{CF}$  which is half of the first vector, gives the

following:

$$r_f = \frac{2\vec{\nabla}\Delta_C.\Delta\vec{r}_{Cf} - \vec{\nabla}\delta_f.\Delta\vec{r}_{Cf}}{\vec{\nabla}\delta_f.\Delta\vec{r}_{Cf}} \tag{27}$$

The node gradient is based on the element shape functions. This gradient reconstruction is based on the method by Tran et al. [35]. This approach uses the element shape functions to determine the vertex gradient. The gradient of a vertex will change for every element that shares the same vertex; therefore a volumetric mean is used to evaluate the gradient at vertex C. In this work, Eqs. (26) and (27) are used together to evaluate the high-resolution scheme. We also investigated two flux-limiters: The MINMOD [36], which is the most diffusive TVD limiter; and the Koren’s limiter [37], which is a very compressive limiter. The expressions used to evaluate both limiters in this work are given by the following.

$$\text{MINMOD} : \psi(r_f) = \max(0, \min(1, r_f)) \tag{28}$$

$$\text{Koren} : \psi(r_f) = \max\left(0, \min\left(2, 2r_f, \frac{r_f + 2}{3}\right)\right) \tag{29}$$

Other forms of flux-limiters also called by slope-limiters are available in the literature [38, 39].

### 5. RESULTS

The first case study presented is one-dimensional water injection displacement. For this case, the parameters were adjusted in such way that the water front profile into the reservoir is exactly a step function. All the reservoir and fluid data for this case are shown in Table 1. This case is described by the Buckley-Leverett equation

**Table 1.** Fluid and reservoir data — case 1

Property	Value
Length, width and thickness	304.8 m, 91.44 m and 6.096 m
Porosity (fraction)	0.15
Water viscosity	$10^{-3} \text{ Pa} \cdot \text{s}$
Oil viscosity	$10^{-3} \text{ Pa} \cdot \text{s}$
Reservoir pressure	34.474 MPa
Water injection rate	$6.22 \times 10^{-4} \text{ m}^3/\text{s}$
Producer’s bottom hole pressure	34.474 MPa
Water initial saturation	0.363
Water residual saturation	0.363
Oil residual saturation	0.25
Water permeability end point	1.0
Oil permeability end point	1.0
Water permeability exponent	1.0
Oil permeability exponent	1.0

and an analytical solution is available [40]. In order to simulate this problem we have used a quadrilateral mesh that allows us to mimic exactly the 1-D fluid flow inside the reservoir. The results are compared in terms of water saturation front at 100 days of simulation. The results of MWU, modified MWU and SUCV schemes are not shown for this case because for the type of grid and fluid flow these schemes are reduced to upwind scheme. Figure 3 presents the results of saturation front obtained with the upwind and the TVD scheme using the MINMOD and Koren flux-limiters with two meshes: one with 100 elements and another one with 2,000 elements.

As one can observe in Figure 3, the Koren’s flux limiter is the more accurate scheme for the methods tested here. Also, we can observe that the front obtained

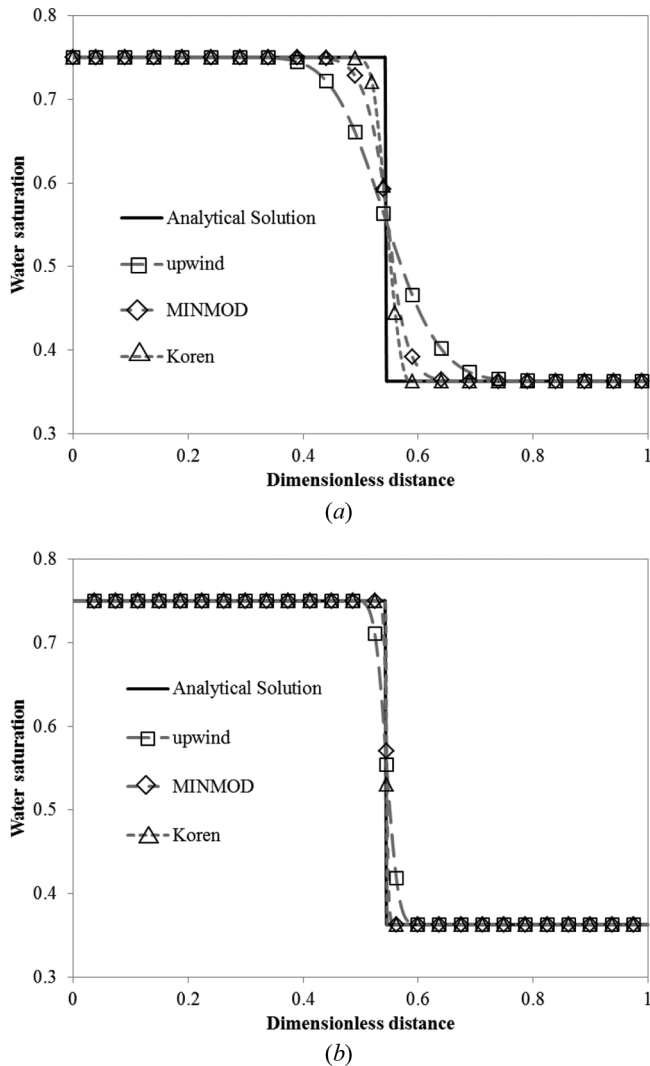


Figure 3. Water saturation front at 100 days — case 1. a) Coarse mesh, and b) refined mesh.

with the coarse mesh using the Kroren’s flux limiter is approximately the same as the one obtained with the upwind scheme using the refined mesh. The  $L_1$  norm for methods investigated is shown in Figure 4, also for 100 days of simulation.

As we can see in Figure 4, the upwind scheme presented the largest errors and an order of accuracy of 0.5019, although this scheme is formally first-order accurate. However, this behaviour is expected, since for problems with discontinuity the observed order for  $L_1$  norm is one half when using upwind the scheme [41]. For second-order and third order schemes, the expected order of the error is 2/3 and 3/4, respectively [41]. Thus, for this case, the MINMOD flux-limiter was second order accurate, and the Koren’s flux-limiter was at least third-order accurate.

For validating the two dimensional flux limiter, a tracer injection case was tested. The reservoir and fluid data are shown in Table 2.

The tracer is injected through water flow until the water injected volume is equal to 0.2 of the reservoir pore volume (PV). Subsequently, no tracer is injected and the water injection continues until 1.6 PV. The analytical solution for this case is presented in reference [42].

Figure 5 presents two triangle grids that were used. These grids are similar to the convectional diagonal and parallel grids commonly employed in petroleum reservoir simulation to verify grid orientation effects. The lower-left and upper-right points in this figure denote the injector and producer wells, respectively. Although the physical solution is independent of mesh configuration, it well known in the literature that these type of meshes are extremely useful for testing interpolation functions. Figure 6a shows the normalized tracer concentration at the producer well comparing all the equal-order schemes, and Figure 6b shows the same for the higher-order scheme. The results are also compared to the analytical solution.

As it can be seen in Figure 6a, for the diagonal grid the MWU was the most accurate scheme, followed by MMWU, SUCV, and upwind schemes. For the parallel grid, however, the best scheme was the SUCV, followed by upwind, MMWU, and

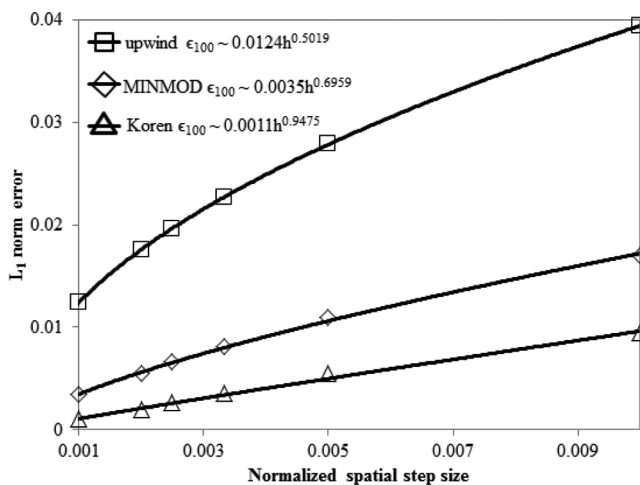


Figure 4.  $L_1$  norm error at 100 days — case 1.

**Table 2.** Fluid and reservoir data — case 2

Property	Value
Length, width and thickness	50.292 m, 50.292 m, and 0.3048 m
Porosity (fraction)	0.2
Water viscosity	$2.49 \times 10^{-4} \text{ Pa} \cdot \text{s}$
Reservoir pressure	13.79 MPa
Water injection rate	20.39 mol/s
Producer's bottom hole pressure	13.79 MPa
Water initial saturation	1.00
Longitudinal dispersion coefficient	0.2012 m
Transversal dispersion coefficient	0.0201 m
Injected tracer's concentration	200 ppm

MWU scheme. However, results from the aforementioned schemes, in general, were not too different, since the order of accuracy may be the same. More importantly, taking into account the computation cost of all the first order schemes, there is no reason to use other first order scheme rather than the upwind scheme. In Figure 6*b*, it can be seen that the TVD using the MINMOD and Koren's flux-limiters was much better than all equal-order schemes tested. Also, for both grids used, the Koren's flux-limiter displaced much less mesh orientation effect than the MINMOD flux-limiter.

The third case study is CO<sub>2</sub> injection flooding. The hydrocarbon mixture is composed of three hydrocarbon components, but only CO<sub>2</sub> and C<sub>1</sub> are injected in a volumetric constant rate into the reservoir. At initial condition, we have a saturated reservoir. All reservoir and fluid data are presented in Table 3.

Two  $40 \times 40$  sets of grids similar to the ones presented in Figure 5 are used here. Figure 7*a* shows the comparison of the oil production rate for the two grids for all equal-order schemes. These results are compared with the fine-grid solution, a randomized triangle grid with 10,114 vertices. Figure 7*b* is similar to Figure 7*a*, but it compares the TVD scheme associated to MINMOD and Koren's flux-limiters. Once again, the results of all investigated interpolations functions were similar to the results presented for case 2.

Figure 8 shows the gas saturation field at 100 days. As the fields for equal order schemes are very similar, only the results for upwind scheme are presented. Figures 8*a*

**Table 3.** Fluid and reservoir data — case 3

Property	Value
Length, width and thickness	170.688 m, 170.688 m, and 30.48 m
Porosity (fraction)	0.3
Water viscosity	$8 \times 10^{-4} \text{ Pa} \cdot \text{s}$
Reservoir pressure	20.68 MPa
Gas injection rate	$6.55 \text{ m}^3/\text{s}$
Producer's bottom hole pressure	20.68 MPa
Water initial saturation	0.25
Reservoir initial compositions (CO <sub>2</sub> , C <sub>1</sub> , C <sub>10</sub> )	0.01, 0.19, 0.80
Injector well composition (CO <sub>2</sub> , C <sub>1</sub> , C <sub>10</sub> )	0.95, 0.05, 0

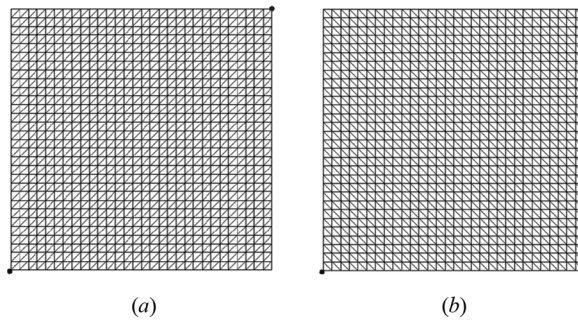


Figure 5. Grids used for case 2. *a*) Parallel configuration, and *b*) diagonal configuration.

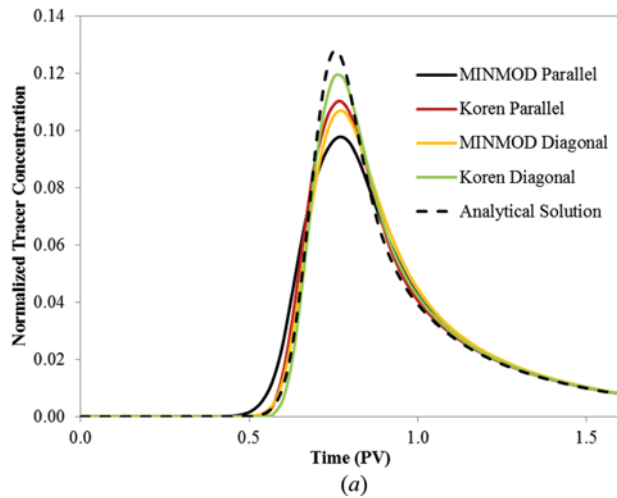
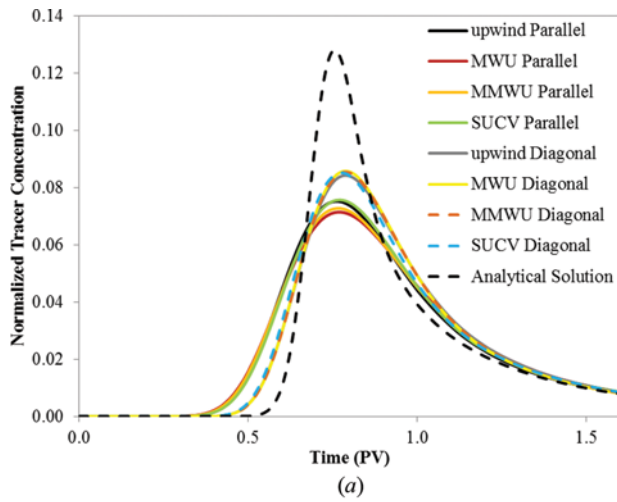
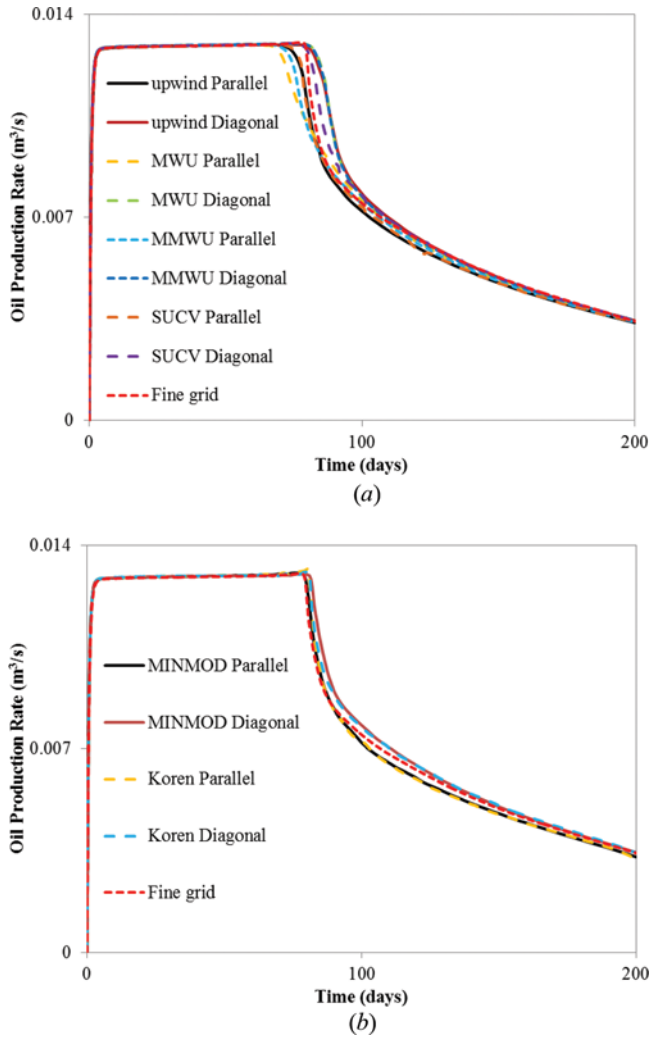


Figure 6. Tracer concentration — case 2. *a*) Equal-order schemes, and *b*) Higher-order schemes (color figure available online).



**Figure 7.** Oil production rate for case study 3. *a*) Equal-order schemes, and *b*) higher-order schemes (color figure available online).

and *8b* show the field for parallel and diagonal grids, respectively, for upwind scheme. Figures *8c* and *8d* show the field for parallel and diagonal grids, respectively, for Koren's scheme. Although, we can observe a large grid orientation effect for both interpolation functions, the solution obtained with TVD and Koren's flux-limiter is much sharper than the one obtained with the upwind scheme.

In order to show the flexibility of the unstructured grids, an irregular reservoir is tested. For this case, 6 components are considered, and gas is injected into wells in the reservoir. All reservoir and fluid data are shown in Table 4.

The gas saturation field at 4,000 days for upwind and TVD scheme with Koren's flux-limiter is shown in Figures *9a* and *9b*, respectively. In Figure 9, one



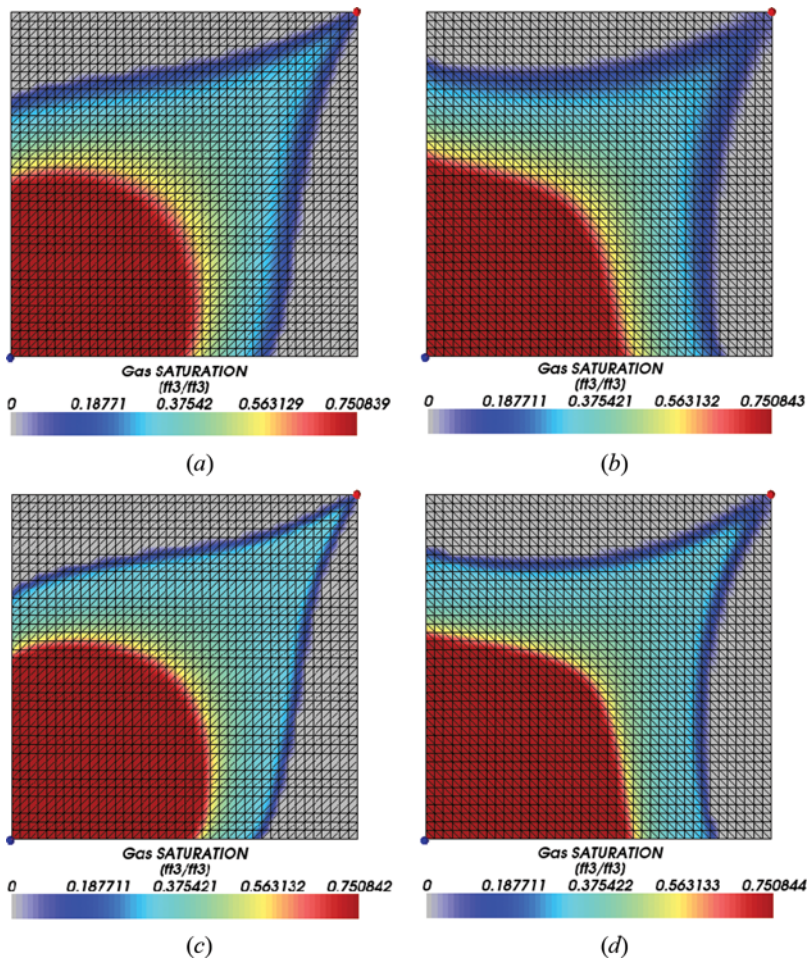


**Figure 8.** Gas saturation field for case study 3. *a)* Upwind parallel, *b)* upwind diagonal, *c)* Koren parallel, and *d)* Koren diagonal (color figure available online).

**Table 4.** Fluid and reservoir data — case 4

Property	Value
Porosity (fraction)	0.35
Water viscosity	$1 \times 10^{-3} \text{ Pa} \cdot \text{s}$
Reservoir pressure	10.34 MPa
Gas injection rate	$0.655 \text{ m}^3/\text{s}$
Producer's bottom hole pressure	8.96 MPa
Water initial saturation	0.17
Reservoir initial compositions ( $C_1, C_3, C_6, C_{10}, C_{15}, C_{20}$ )	0.5, 0.03, 0.07, 0.2, 0.15, 0.05
Injector well composition ( $C_1, C_3, C_6, C_{10}, C_{15}, C_{20}$ )	0.77, 0.20, 0.01, 0.01, 0.005, 0.005

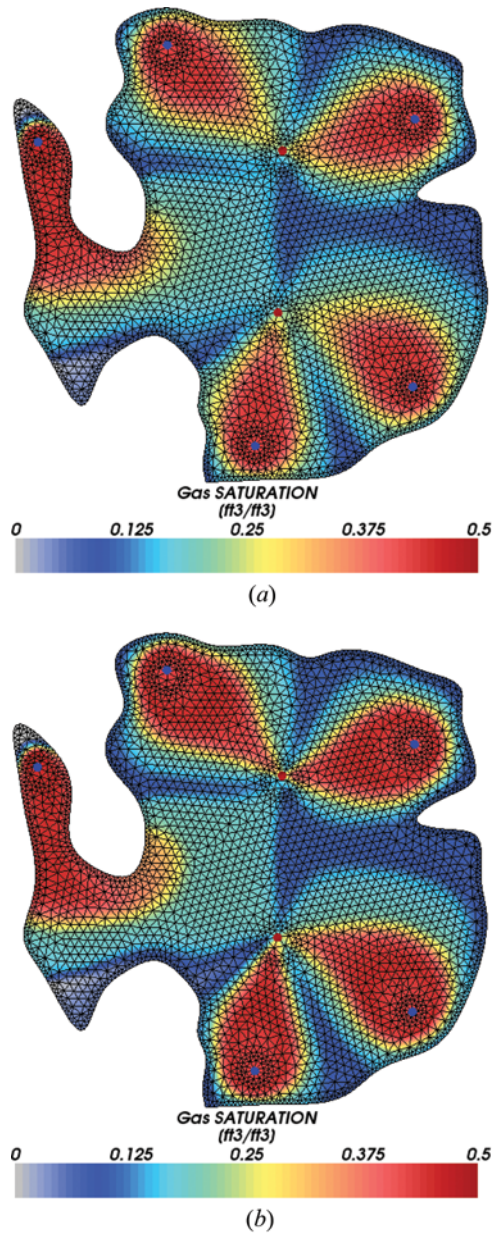


**Figure 9.** Gas saturation field for case study 4. *a*) Upwind, and *b*) TVD with Koren's flux-limiter (color figure available online).

can observe that the solution obtained with TVD and Koren's flux-limiter is much more compressive than the one obtained with upwind scheme, as expected. Even using an irregular geometry, the TVD approach is a much better choice since the saturation gradients are better captured, as can be seen in Figure 9.

## 7. CONCLUSION

We presented the implementation of MWU, MMWU, SUCV, and a TVD scheme using MINMOD and Koren flux-limiters in conjunction with petroleum reservoir simulation using cell-vertex unstructured meshes. The TVD implementation was adapted to EbFVM approach. The results of presented case studies were validated with available analytical solutions. The results suggested that the SUCV is more accurate than the upwind for the cases presented. The MWU and MMWU showed grid dependence on the accuracy. For the TVD scheme in conjunction with unstructured grids, it was found that the scheme can produce numerical solution as accurate as the ones for structured grids. For the other cases, both MINMOD and Koren's flux limiters were far more accurate than the other first order schemes investigated.

## REFERENCES

1. B. R. Baliga and S. V. Patankar, A New Finite-Element Formulation for Convection-Diffusion Problems, *Numer. Heat Transfer*, vol. 3, no. 4, pp. 393–409, 1980.
2. C. Prakash, An Improved Control Volume Finite-Element Method for Heat and Mass Transfer, and for Fluid Flow using Equal-Order Velocity-Pressure Interpolation, *Numer. Heat Transfer*, vol. 9, no. 3, pp. 253–276, 1986.
3. G. D. Raithby, A Critical Evaluation of Upstream Differencing Applied to Problems Involving Fluid Flow, *Computer Methods in Appl. Mech. and Eng.*, vol. 9, no. 1, pp. 75–103, 1976.
4. G. D. Raithby, Skew Upstream Differencing Schemes for Problems Involving Fluid Flow, *Computer Methods in Appl. Mech. and Eng.*, vol. 9, no. 2, pp. 153–164, 1976.
5. Y. A. Hassan, J. G. Rice, and J. H. Kim, A Stable Mass-Flow-Weighted Two-Dimensional Skew Upwind, *Numer. Heat Transfer*, vol. 6, no. 4, pp. 395–408, 1983.
6. G. E. Schneider, M. J. Raw, and A Skewed, Positive Influence Coefficient Upwinding Procedure for Control-Volume-Based Finite-Element Convection-Diffusion Computation, *Numer. Heat Transfer*, vol. 9, no. 1, pp. 1–26, 1986.
7. C. Masson, H. J. Saabas, and B. R. Baliga, Co-Located Equal-Order Control-Volume Finite-Element Method for Two-Dimensional Axisymmetric Incompressible Fluid Flow, *Int. J. for Numer. Methods in Fluids*, vol. 18, no. 1, pp. 1–26, 1994.
8. H. J. Saabas and B. R. Baliga, Co-Located Equal-Order Control-Volume Finite-Element Method for Multidimensional, Incompressible, Fluid Flow — Part I: Formulation, *Numer. Heat Transfer, B*, vol. 26, no. 4, pp. 381–407, 1994.
9. H. J. Saabas and B. R. Baliga, Co-Located Equal-Order Control-Volume Finite-Element Method for Multidimensional, Incompressible, Fluid Flow — Part II: Verification, *Numer. Heat Transfer B*, vol. 26, no. 4, pp. 409–424, 1994.
10. C. R. Swaminathan and V. R. Voller, Streamline Upwind Scheme for Control-Volume Finite Elements, Part I: Formulations, *Numer. Heat Transfer B*, vol. 22, no. 1, pp. 95–107, 1992.
11. C. R. Swaminathan and V. R. Voller, Streamline Upwind Scheme for Control-Volume Finite Elements, Part II: Implementation and Comparison with the SUPG Finite-Element Scheme, *Numer. Heat Transfer B*, vol. 22, no. 1, pp. 109–124, 1992.
12. B. van Leer, Towards the Ultimate Conservative Difference Scheme, V — A Second-Order Sequel to Godunov's Method, *J. of Computational Physics*, vol. 32, no. 1, pp. 101–136, 1979.
13. A. Harten, High Resolution Schemes for Hyperbolic Conservation Laws, *J. of Computational Physics*, vol. 49, no. 3, pp. 357–393, 1983.

14. P. K. Sweby, High Resolution Schemes using Flux Limiters for Hyperbolic Conservation Laws, *SIAM J. on Numer. Analysis*, vol. 21, no. 5, pp. 995–1011, 1984.
15. P. L. Roe, Some Contributions to the Modelling of Discontinuous Flows, In *Lecture Notes in Applied Mathematics*, 22, pp. 349–359, Springer, New York, 1991.
16. S. R. Chakravarthy and S. Osher, High Resolution Applications of the Osher Upwind Scheme for the Euler Equations, Computational Fluid Dynamics, *Proc. of the 6th Computational Fluid Dynamics Conf.*, pp. 363–372, Danvers, USA, 1983.
17. P. Lax and B. Wendroff, Systems of Conservation Laws, *Comm. on Pure and Appl. Mathematics*, vol. 13, no. 2, pp. 217–237, 1960.
18. R. F. Warming and R. M. Beam, Upwind Second Order Difference Schemes, and Applications in Aerodynamics, *AIAA J.*, vol. 14, no. 9, pp. 1241–1249, 1976.
19. C. W. S. Bruner and R. W. Walters, Parallelization of the Euler Equations on Unstructured Grids, *AIAA* paper 97-1894, 1995.
20. C. W. S. Bruner, Parallelization of the Euler Equations on Unstructured Grids, Ph.D. Dissertation, Virginia Polytechnic Institute and State University, Department of Aerospace Engineering, 1996.
21. M. S. Darwish and F. Moukalled, TVD Schemes for Unstructured Grids, *Int. J. of Heat and Mass Transfer*, vol. 46, no. 4, pp. 599–611, 2003.
22. C. M. Rhie and W. L. Chow, Numerical Study of the Turbulent Flow Past and Airfoil with Trailing Edge Separation, *AIAA J.*, vol. 21, no. 11, pp. 1525–1532, 1983.
23. C. O. E. Burg, High-Order Variable Extrapolation for Unstructured Finite Volume RANS Solvers, AIAA paper 2005-4999, AIAA Computational Fluid Dynamics 2005, *17th AIAA Computational Fluid Dynamics Conference*, Toronto, Canada, 2005.
24. L. Li, H. Liao, and L. Qi, An Improved r-Factor Algorithm for TVD Schemes, *Int. J. of Heat and Mass Transfer*, vol. 51, no. 3–4, pp. 610–617, 2008.
25. J. Hou, F. Simons, and R. Hinkelmann, Improved Total Variation Diminishing Schemes for Advection Simulation on Arbitrary Grids, *Int. J. for Numer. Methods in Fluids*, vol. 70, no. 3, pp. 359–382, 2011.
26. J. Hou, F. Simons, and R. Hinkelmann, A New TVD Method for Advection Simulation on 2-D Unstructured Grids, *Int. J. for Numer. Methods in Fluids*, vol. 71, no. 10, pp. 1260–1281, 2013.
27. Y.-B. Chang, Development and Application of an Equation of State Compositional Simulator, Ph.D. thesis, The University of Texas at Austin, Department of Petroleum and Geosystems Engineering, 1990.
28. Y.-B. Chang, G. A. Pope, and K. Sepehrnoori, A Higher Order Finite-Difference Compositional Simulator, *J. of Petroleum Sci. & Eng.*, vol. 5, no. 1, pp. 35–50, 1990.
29. G. Ács, S. Doleschall, and E. Farkas, General Purpose Compositional Model, *SPE J.*, vol. 25, pp. 543–553, 1985.
30. J. Cordazzo, An Element Based Conservative Scheme using Unstructured Grids for Reservoir Simulation, SPE International Student Paper Contest, *SPE Annual Technical Conference and Exhibition*, Houston, USA, 2004.
31. F. Marcondes and K. Sepehrnoori, Unstructured Grids and an Element Based Conservative Approach for Compositional Reservoir Simulation, *The 19th Int. Congress of Mechanical Eng.*, Brasília, Brazil, 2007.
32. F. Marcondes and K. Sepehrnoori, An Element-Based Finite Volume-Method Approach for Heterogeneous and Anisotropic Compositional Reservoir Simulation, *J. of Petroleum Sci. & Eng.*, vol. 73, no. 1–2, pp. 99–106, 2010.
33. H.-T. Chiu and L. J. Lee, Simulation of Liquid Composite Molding based on Control-Volume Finite Element Method, *J. of Polymer Eng.*, vol. 22, no. 3, pp. 155–175, 2002.

34. D. R. Rousse and S. Lassue, A Skew Upwinding Scheme for Numerical Radiative Transfer, Advances in Computational Heat Transfer 2008, *Int. Symp. On Advances in Computational Heat Transfer*, Marrakech, Marrocco, 2008.
35. L. D. Tran, C. Masson, and A. Smaïli, A Stable Second-Order Mass-Weighted Upwind Scheme for Unstructured Meshes, *Int. J. for Numer. Methods in Fluids*, vol. 51, no. 7, pp. 749–771, 2006.
36. P. L. Roe, Some Characteristic-Based Schemes for the Euler Equations, *Ann. Rev. of Fluid Mechanics*, vol. 18, pp. 337–365, 1986.
37. B. Koren, A Robust Upwind Discretization Method for Advection, Diffusion and Source Terms, in C. B. Vreugdenhil and B. Koren (eds.), *Numerical Methods for Advection-Diffusion Problems*, Notes on Numerical Fluid Mechanics, vol. 45, pp. 117–138, Vieweg, Braunschweig, 1993.
38. M. Berger, M. J. Aftomis, and S. M. Murman, Analysis of Slope Limiters on Irregular Grids, AIAA Aerospace 2005, *43rd AIAA Aerospace Meeting*, Reno, NV, USA, 2005.
39. B. F. Sanders and S. F. Bradford, Impact of Limiters on Accuracy of High-Resolution Flow and Transport Models, *J. of Eng. Mechanics*, vol. 132, no. 1, pp. 87–98, 2006.
40. S. E. Buckley and M. C. Leverett, Mechanism of Fluid Displacement in Sands, *Tran. of the ASME*, vol. 146, pp. 107–116, 1942.
41. C. Zoppou and S. Roberts, Behaviour of Finite Difference Solution of the Advection Equation, Technical Report MRR 062–96, School of Mathematical Sciences, Australian National University, Canberra, Australia, 1996.
42. M. Abbaszadeh-Dehghani and W. E. Brigham, Analysis of Well-to-Well Tracer Flow to Determine Reservoir Layering, *J. of Petroleum Tech.*, vol. 36, pp. 1753–1762, 1984.